A Dynamical Study of the $Si^+ + H_2O$ Reaction

Jesús R. Flores*

Departamento de Química Física, Facultad de Química, Universidad de Vigo, E-36200 Vigo, Spain

Received: July 12, 2007; In Final Form: August 17, 2007

A dynamical study of the $Si^+ + H_2O$ reaction has been carried out by means of a quasiclassical trajectory method that decomposes the reaction into a capture step, for which an accurate analytical potential is employed, and an unimolecular step, in which the evolution of the collision complex is studied through a direct dynamics BHandHLYP/6-31G(d,p) method. The capture rate coefficient has been computed for thermal conditions corresponding to temperatures ranging from 50 to 1000 K. It is concluded that the main reason why the reaction rate is about 10 times smaller than the capture rate (at $T = 298$ K) is the topology of the potential energy surface of the ground state. It is also concluded that the ratio between the rates of product and reactant generation from the collision complex decreases quite steeply with increasing temperature, and therefore, the reaction rate decreases even more sharply. Exciting the stretching normal modes of water substantially increases that ratio, and moderate rotational excitation does not appear to have a relevant effect. The collision complex is always initially $SiOH_2^+$, but in some trajectories, it becomes $HSiOH^+$, which generates the products, although the former species is the main intermediate.

1. Introduction

The reaction of Si^+ with water is believed to be of some relevance in the depletion of Si^+ in the earth's atmosphere.[1] It could also be responsible for the production of SiO in interstellar space through the following reaction scheme

$$Si^+ + H_2O \rightarrow SiOH^+ + H$$

$$SiOH^+ + e^- \rightarrow SiO + H$$

which would be complementary to that initiated by the $SiO^+ + H_2 \rightarrow SiOH^+ + H$ reaction.[2−4]

The title reaction has been studied by experiment through the selected ion flow tube technique. Fahey et al. have employed a selected ion flow drift tube (SIFDT) apparatus to determine the rate coefficient at room temperature using He buffer gas at about 0.5 Torr and obtained a value of $2.3 \pm 0.9 \times 10^{-10}$ cm^3 s^{-1} for $T = 300$ K.[1] Wlodek et al. have used a SIFT apparatus and have obtained the same value for the rate constant with an error of ±30%.[5] They have also reported a theoretical capture rate of 2.7×10^{-9} cm^3 s^{-1} (at $T = 296$ K), which they obtained using Su and Chesnavich's method, which employs a charge dipole + charge-induced dipole potential.[6] Glosík et al.[7] have used a SIFDT apparatus to determine the rate coefficient as a function of the reactant's collision center-of-mass kinetic energy (KE_{CM}), also using He as a buffer gas at 298 ± 2 K. They observed that the rate coefficient decreases quite sharply with increasing KE_{CM}.

The present author has performed an ab initio study of the potential energy surface (PES) of the $SiOH_2^+$ and $SiOH^+$ systems using a modified Gaussian 1 procedure, which showed that the only product for which the $Si^+ + H_2O$ reaction is exothermic is $SiOH^+ + H$; the formation of $SiO^+ + H_2$ and, especially, that of the other isomer $HSiO^+ + H$ are endothermic processes. González, Clary, and Yáñez have recomputed the most relevant stationary points of the $SiOH_2^+$ PES at the Gaussian 2 level and have performed an adiabatic capture centrifugal sudden approximation (ACCSA) computation of the capture process involved in title reaction, which gave a value of 2.3×10^{-9} cm^3 s^{-1},[8] which is only slightly smaller than Wlodek's value[5] and still 10 times larger than the reaction rate. On the basis of the difference with respect to the behavior of the $C^+ + H_2O$ reaction, they hypothesized that the dramatic discrepancy between the capture and the experimental rates must be due to the topology of the $SiOH_2^+$ PES.

The reaction of atomic ions and polar molecules at low-energy conditions usually involves dipole alignment; therefore, in the present case, the region of the PES corresponding to a XOH_2^+ complex (i.e., a species with an X−O bond) would be first visited. This hypothesis has been confirmed in the case of the $C^+ + H_2O$ reaction by the quasiclassical trajectory computations of Ishikawa et al.,[9,10] who have used a direct dynamics approach, and by the present author, who has employed a finite element method (FEM) representation of the potential surface obtained with a geometry-dependent density functional method.[11] It is often the case that ion−molecule reactions take place at a rate close to the capture value, provided the latter is corrected by an electronic factor which represents the ratio between the number of electronic states which become attractive at short ion−molecule distances and the total number of electronic states.[12] However, it is quite natural to suspect that the reaction rate could get much smaller than the capture rate if the fragmentation of the XOH_2^+ complex into the products, or its isomerization into other species which may undergo fragmentation more easily, implies saddle points which lie quite high, meaning that they are close in energy to the reactants, even if the reaction has no potential energy barrier.

The purpose of the present work is twofold. First, we have intended to determine whether the low rate of the $Si^+ + H_2O$ reaction can be attributed to the topology of the potential energy surface of the electronic ground state and, as much as possible, to quantify that effect. And second, we have tried to provide

* To whom correspondence should be addressed. E-mail: flores@uvigo.es.

10.1021/jp075439t CCC: $37.00
Published on Web 10/11/2007

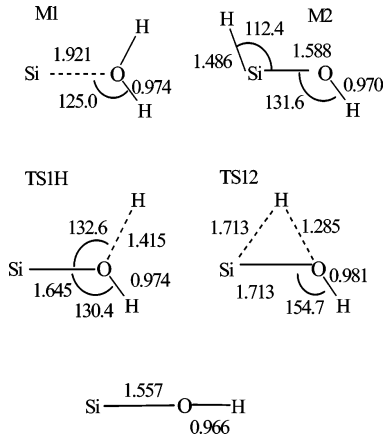

Figure 1. MP2(full)/6-31G(d,p)-optimized geometries of the most relevant minima and saddle points (Å and degrees).

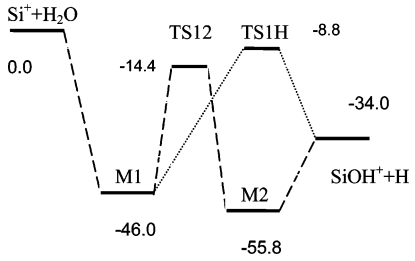

Figure 2. Simplified mechanistic scheme of the $Si^+ + H_2O \rightarrow SiOH^+ + H$ reaction. The numbers indicate G3(0 K) energy differences in kcal/mol with respect to the reactants. M2 is in its trans form. The G1*(0 K) values are, in kcal/mol, −46.8 (M1), −56.2 (M2), −33.8 ($SiOH^+ + H$), −16.3 (TS12), and −10.9 (TS1H).

some information about the dependency of the rate constant with temperature, with the relative translational energy of the collision, and with the vibrational or rotational excitation, which may be of interest in atmospheric chemistry and astrophysics.

2. Computational Methods

2.A. Computation of the PES. *2.A.1. The Computation of the PES of the $SiOH_2^+$ System.* The PES of the $SiOH_2^+$ system in its ground state was computed quite accurately some time ago by means of a modified Gaussian 1 method, which we will denote as (G1*);[13] we have updated those computations to the Gaussian 3 level.[14] Basically, there are four local minima, $SiOH_2^+(^2B_2)$ (M1), $HSiOH^+(^2A')$ which presents cis and trans forms ($M2_c$ and $M2_t$), $H_2SiO^+(^2B_2)$, and a loosely bound ion−molecule complex SiO^+-H_2. Under the conditions considered in the present work (low excitation energy of the reactants), $SiOH^+(^1\Sigma^+) + H(^2S)$ is the only product, and the important section of the PES includes the minima M1 and M2 and the saddle points TS1H and TS12. Production of $SiOH^+$ from M2 has no saddle point. The important structures are depicted in Figure 1. A reaction scheme is presented in Figure 2. As we have pointed out in the Introduction and as will be discussed further in section 3, the behavior of the electronic states for decreasing Si^+-OH_2 distances, that is, whether they are attractive or repulsive, can be a crucial aspect in the reaction dynamics. It turns out that there are three electronic states which become degenerate at long Si^+-H_2O distances. In C_{2v} symmetry, they are labeled $^2B_2$, $^2B_1$, and $^2A_1$. Figure 3 presents energy profiles computed at the AQCC/aug-cc-pVTZ level[15−17] on geometries of a reaction coordinate obtained by minimizing the MP2/aug-cc-pVTZ energy of the $^2B_2$ state for varying Si−O distances (Si^+-OH_2) within C_{2v} symmetry. The orbitals em-

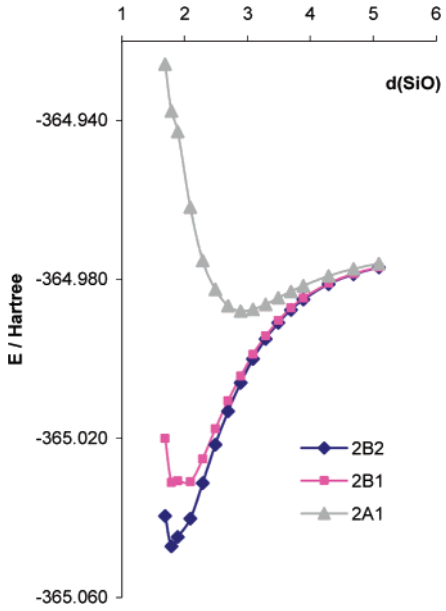

Figure 3. Energy profiles for the three nearly degenerate electronic states of the reactants as a function of the Si^+-OH_2 distance computed at the AQCC/aug-cc-pVTZ level in a MP2/aug-cc-pVTZ reaction coordinate.

ployed in the AQCC (multireferenced averaged quadratic coupled-cluster method) computations have been obtained in a (complete active space) CAS-type state-averaged MCSCF computation[18,19] of the three electronic states with the following set of active orbitals: $\{(4-9)a_1,(2-3)b_1,(2-4)b_2\}$. It is readily seen that the $^2B_2$ and $^2B_1$ states are neatly attractive, whereas the $^2A_1$ state becomes repulsive at approximately $d(Si-O) = 2.4$ Å. The $^2B_1-^2B_2$ energy gap is only 8.3 kcal/mol at $d(Si-O) = 1.891$ Å.

The AQCC/aug-cc-pVTZ computations have been performed with the MOLPRO 2002 program.[20]

2.A.2. The Selection of the Electronic Structure Method for the Direct Dynamics Trajectories. In order to perform a direct dynamics computation, one has to select an electronic structure method that is both reasonably accurate and "economical" in terms of computer resources. The task is not particularly easy. Ab initio methods based on unrestricted Hartree−Fock wave functions suffer from spin contamination problems, which make them unreliable not only because of the spin contamination itself but also because of the possible appearance of multiple solutions of the Hartree−Fock equations. Density functional theory offers an interesting alternative, but the need to describe the long-range part of the PES reasonably well and the existence of nearly ionic bonds makes the choice of the density functional nontrivial in the case of ion−molecule reactions. Rather than relying on the DFT method to describe the interaction between Si^+ and H_2O at the very long range, we have used an analytical potential for that purpose. The trajectory has been split into two parts; the first employs the analytical potential, whereas the second involves direct dynamics[21] with the DFT method. Alternatively, one can view the first part of the trajectory as the sampling step of the direct dynamics computation.

We have tried the B3LYP[22] and half-and-half LYP (BHandHLYP)[23] functionals with a variety of basis sets and have selected the BHandHLYP/6-31G(d,p)[23−25] level as the optimum compromise between the degree of accuracy provided and the need of resources. For comparison, we include in Table 1 the results of the DFT levels, which provide reasonably good values. The aspect that we have considered to be more crucial is the position

TABLE 1: Electronic Energy Differences (kcal/mol) $\Delta E = [E(X) - E(Si^+ + H_2O)]_{DFT} - [E(X) - E(Si^+ + H_2O)]_{G3}$ for the Stationary Points of the Ground-State PES of the $SiOH_2^+$ System, Which Are the Most Important in the Dynamics of the $Si^+ + H_2O$ Reaction[a]

level[b]	M1	M2	TS1H	TS12	$SiOH^+(^1\Sigma^+) + H$
BHandHLYP/6-31G(d,p)	−5.1	−0.3	0.7	1.7	4.6
BHandHLYP/6-311G(d,p)	−3.8	0.9	1.3	2.4	4.6
BHandHLYP/6-311++G(3df,2p)	0.3	−1.0	2.8	2.0	4.2
BHandHLYP/cc-pVDZ	−5.2	3.8	2.1	1.9	7.3
B3LYP/6-31G(d,p)	−6.9	−3.4	−9.5	−6.2	1.3
B3LYP/6-311G(d,p)	−5.3	−1.8	−8.5	−4.9	1.4
B3LYP/6-311++G(3df,2p)	0.1	−1.7	−5.4	−3.3	2.8
B3LYP/cc-pVDZ	−7.6	−1.0	−9.4	−7.0	2.3

[a] The $[E(X) - E(Si^+ + H_2O)]_{G3}$ electronic energy differences are (in kcal/mol) −47.6 (M1), −55.0 (M2), −5.1 (TS1H), −10.9 (TS12), and −28.9 ($SiOH^+(^1\Sigma^+) + H$). [b] The geometries employed are optimal for the corresponding level, that is, B3LYP/cc-pVDZ means B3LYP/cc-pVDZ//B3LYP/cc-pVDZ.

TABLE 2: Capture Rate Coefficients for Several Temperatures in Units of 10^{-9} cm^3 s^{-1} and Statistical Errors[33]

T	k_c
50.00	3.86(9)
100.00	3.57(13)
150.00	3.49(15)
200.00	3.18(16)
250.00	2.83(17)
298.15	2.61(17)
400.00	2.29(18)
500.00	2.04(18)
650.00	1.90(19)
800.00	1.71(19)
1000.00	1.7(2)

of saddle points TS12 and TS1H with respect to the reactants and relative to each other because, as we will see, we want to correctly describe the competition between two processes, (i) dissociation back to the reactants ($SiOH_2^+ \rightarrow Si^+ + H_2O$) and (ii) fragmentation or isomerization of the intermediate ($SiOH_2^+ \rightarrow SiOH^+ + H$, $SiOH_2^+ \rightarrow HSiOH^+ \rightarrow SiOH^+ + H$). It is readily seen that the BHandHLYP/6-311G(d,p) method provides a good description, but it turns out to be already a little too expensive in terms of computer time; therefore, we have selected the BHandHLYP/6-31G(d,p) method. It should also be noted that a rather large basis set such as 6-311++G(3df,2p),[26] which, in any case, would be prohibitively expensive to use, does not provide better results for the relative energy of TS12 and TS1H with respect to the reactants, although it gives rather good values for M1 and M2. Indeed, the selected method (BHandHLYP/6-31G(d,p)) has the shortcoming of providing too large TS1H-M1 or TS12-M1 energy differences. The computations mentioned in the present section as well as the MP2/aug-cc-pVTZ computations of the former section were performed with the Gaussian 03 program package.[23]

2.A.3. The Long-Range Analytical Potential. The long-range potential is constructed from several components

$$V_{l-r} = V_r + V_q + V_L + V_i \qquad (1)$$

where V_q represents the charge−dipole potential, V_r is a repulsive part important at short distances, V_L contains a further attractive term, and V_i is an internal potential for water, which is modulated according to the Si−O distance. The present analytical potential is designed in the spirit of the work by Vande Linde and Hase.[27] Appendix A describes it in more detail, whereas the values of the many parameters are shown in the Supporting Information. The parameters have been obtained by fitting to a set of energy data obtained at the MP2 level with the aug-cc-pVTZ[17] and 6-311++G(2df,p)[26] basis sets for varying Si−O distances and water orientations and geometries, as well as with the help BHandHLYP/6-31G(d,p) computations of isolated water. The potential is intended to be a good description of the system for $d(Si-O) > 3.5$ Å.

2.B. The Integration of the Equations of Motion. We distinguish two types of trajectories, those included in the study of the capture rate and those employed to analyze the behavior of the collision complex. In the first case, we have used the long-range potential, in other words, we have not employed direct dynamics at all. In the other case, each trajectory has been divided into long- and short-range parts. Initial conditions have been set at the long range, and the trajectory has been integrated up to $d(SiO) = 10.4$ Å with the analytical potential. We have employed the Hase group's Venus 96 program[28−30] to generate the initial conditions according to several sampling procedures. The trajectories used for the capture computation and the long-range part of those employed in the analysis of the collision complex have been integrated by means of the adaptive-step fifth-order Cash−Karp Runge−Kutta method as described in ref 31. The latter kind of trajectory is continued with the direct dynamics code integrated in the Gaussian 03 program package.[32]

3. Results

3.A. The capture Step. As we pointed out in the Introduction, the title reaction can be viewed as a two-step process. The first step involves capture of water by Si^+, that is, the formation of an ion−molecule complex. The second step involves the fragmentation of that complex, either back to the reactants or forward to the products ($SiOH^+(^1\Sigma^+) + H$).

One can consider the first step fulfilled when the centrifugal barrier is passed; for the present reaction, a moderately short Si−O distance of about (4.0 Å) is well past the centrifugal barrier in any of the trajectories considered. In all trajectories reaching that point, basically, dipole locking takes place, that is, water orients, and its rotation contributes to the rovibrational energy of the collision complex ($SiOH_2^+$).

The capture rate constant can be computed as follows

$$k_c(\{T\}) = \int_0^\infty k_c(\epsilon_r;T_{vr})\, f(\epsilon_r;T)\mathrm{d}\epsilon_r \qquad (2)$$

where $\{T\}$ signals the dependence with respect to the temperatures of the distribution functions, $f(\epsilon_r;T)$ is typically the Boltzmann distribution of the relative translational energy ϵ_r, and the energy-dependent capture rate coefficient can be expressed as follows

$$k_c(\epsilon_r;T_{vr}) = \sum_{j,n} k_c(\epsilon_r,\{j,n\}) f_{vr}(\{j,n\};T_{vr}) \qquad (3)$$

where $k_c(\epsilon_r,\{j,n\})$ is the specific capture rate constant for a particular rotation−vibration state $\{j,n\}$ of the molecular reactant

and $f_{vr}(\{j,n\};T_{vr})$ is the corresponding population function, typically a Boltzmann distribution depending on the vibration−rotation temperature. Alternatively, one can simply make the following assignment: $k_c(\epsilon_r) = k_c(\epsilon_r,\{j,n\})$, that is, the molecular reactant could be selected in a particular vibration−rotation state. The state-specific capture rate can be expressed as the product of the relative speed and the capture cross section

$$k_c(\epsilon_r,\{j,n\}) = (2/\mu)^{1/2}\epsilon_r^{1/2}\sigma(\epsilon_r,\{j,n\}) \quad (4)$$

where the capture cross section can be written as[33]

$$\sigma(\epsilon_r,\{j,n\}) = \int \mathrm{d}\rho\ \rho(\{q_i\},\{\theta_i\},\{j,n\}) \int_0^\infty 2\pi b P(\epsilon_r,b,\{q_i\},\{\theta_i\},\{j,n\})\mathrm{d}b \quad (5)$$

$P(\epsilon_r,b,\{q_i\},\{\theta_i\},\{j,n\})$ is the capture probability, b is the impact parameter, and the outer integration corresponds to all geometrical variables of the molecular reactant. The cross section can be rewritten in terms of a maximum impact parameter as $\sigma(\epsilon_r,\{j,n\}) = \pi b_{max}^2 P_\sigma(\epsilon_r,\{j,n\})$, where $P_\sigma(\epsilon_r,\{j,n\})$ is a capture probability function. Introducing the latter expression into eqs 2−4, we get

$$k_c(\{T\}) = \langle\nu\rangle_T \pi b_{max}^2 \int_0^\infty P(\epsilon_r;T)\mathrm{d}\epsilon_r \sum_{j,n} f_{vr}(\{j,n\};T_{vr}) P_\sigma(\epsilon_r,\{j,n\}) \quad (6)$$

where $P(\epsilon_r;T) = (kT)^{-2}\epsilon_r e^{-\epsilon_r/kT}$ and $\langle\nu\rangle_T$ is the average relative speed.

In the context of trajectory computations, the initial values of the geometrical variables and the atomic velocities are sampled through several procedures, depending on the particular distribution to be used;[33] as said above, we have employed the procedures described in ref 28 through the VENUS 96 program. The distributions $P(\epsilon_r;T)$ and $f_{vr}(\{j,n\};T_{vr})$ are sampled so that the capture rate can be computed as

$$k_c(\{T\}) = \langle\nu\rangle_T \sigma_c = \langle\nu\rangle_T \pi\, b_{max}^2\, f_c \quad (7)$$

where σ_c is the total capture cross section and f_c is the ratio of trajectories that lead to capture, that is, $f_c = N_c/N_t$.

One can scale $k_c(\{T\})$ by the electronic factor $f_e = 2/3$, which is the ratio of attractive PESs in the Si^+/H_2O interaction; we consider $f_e k_c$ to be the best approximation to the capture rate.

Table 2 shows computed capture rates $k_c(\{T\})$ for several temperatures from 50 to 1000 K ($T = T_{vr}$), together with the errors associated to the sampling procedure.[33] For each temperature, 1000 trajectories have been run using the thermal sampling procedure implemented in VENUS 96, in combination with the analytical long-range potential of section 2.A. Trajectories leading to capture have been stopped at $d(Si-O) = 4$ Å, well past any centrifugal barrier. As one would expect,[34] the capture rate has a negative temperature dependence; a simple fitting of the type $k_c(T) = A + B/T^m$ leads to an optimal exponent $m = 0.8$. The capture rate at 298 K ($2.61(17) \times 10^{-9}$ cm^3 s^{-1}) is quite close to the ACCSA value of 2.3×10^{-9} cm^3 s^{-1} of González et al. and even closer to the value of Wlodek et al. (2.7×10^{-9} cm^3 s^{-1});[5,6] therefore, all values are at least 10 times larger than the experimental reaction rate (0.23 ± 0.09) $\times 10^{-9}$ cm^3 s^{-1}.[1,5] Of course, scaling by $f_e = 2/3$ does not change the picture.

3.B. The Reaction Rate. The reaction can be schemed as follows

$$\begin{array}{ccccc} Si^+ + H_2O & \underset{k_{-1}}{\overset{k_1}{\rightleftarrows}} & (SiOH_2^+)^* & \xrightarrow{k_2} & SiOH^+ + H \\ & & k_{-3}\uparrow\downarrow k_3 & & \\ & & (HSiOH^+)^* & \xrightarrow{k_4} & SiOH^+ + H \end{array}$$

The rate coefficients can be formulated as dependent on the total energy and total angular momentum. Considering, for simplicity, only the total energy as a variable, we have

$$k_r(\{T\}) = \sum_0^\infty k_1(\epsilon;\{T\}) \frac{k_2(\epsilon) + k_4(\epsilon)r(\epsilon)}{k_{-1}(\epsilon) + k_2(\epsilon) + k_4(\epsilon)r(\epsilon)}\mathrm{d}\epsilon$$

$$r(\epsilon) = k_3(\epsilon)/(k_{-3}(\epsilon) + k_4(\epsilon)) \quad (8)$$

where $k_4(\epsilon)r(\epsilon)$ can be viewed as the rate of decomposition of $(SiOH_2^+)^*$ through the other intermediate $(HSiOH^+)^*$; $k_1(\epsilon;\{T\})$ can be related to the capture rate dependent on the relative translational energy ϵ_r through the following expression

$$k_1(\epsilon;\{T\}) = \int_0^{\epsilon-\epsilon_0} f(\epsilon_r;T)\mathrm{d}\epsilon_r \sum_{j,n} k_c(\epsilon_r,\{j,n\})\, f_{vr}(\{j,n\};T_{vr})\, \delta(\epsilon_{vr}\{j,n\} - (\epsilon - \epsilon_r)) \quad (9)$$

Note that $k_1(\epsilon;\{T\})$ depends on the translation and vibration−rotation temperatures through the distribution functions $f(\epsilon_r;T)$ and $f_{vr}(\{j,n\};T_{vr})$, respectively, $\epsilon_{vr}\{j,n\}$ is the vibration−rotation energy of water, and ϵ_0 is its zero-point value.

The analysis of trajectories reaching $HSiOH^+$ indicates that isomerization back into $SiOH_2^+$ rarely happens, the usual outcome being fragmentation into the products; therefore, $r(\epsilon)k_4(\epsilon) \approx k_3(\epsilon)$.

By reversing the order of the summation over the rovibrational states and integrating over ϵ_r in eq 9, we get the following expression

$$k_1(\epsilon;\{T\}) = \sum_{\substack{j,n \\ \epsilon_{vr}\le\epsilon}} k_c(\epsilon - \epsilon_{vr}(\{j,n\}))\, f_{vr}(\{j,n\};T_{vr})\, f(\epsilon - \epsilon_{vr}(\{j,n\});T) \quad (10)$$

If we define $F(\epsilon) = (k_2(\epsilon) + k_4(\epsilon)r(\epsilon))/(k_{-1}(\epsilon) + k_2(\epsilon) + k_4(\epsilon)r(\epsilon))$ and proceed as in section 3.A, we get

$$k_r(\{T\}) = \langle\nu\rangle_T \pi b_{max}^2 \sum_{j,n} \int_0^\infty P(\epsilon_r;T)\, f_{vr}(\{j,n\};T_{vr})\, P_\sigma(\epsilon_r;\{j,n\})F(\epsilon_{vr}(\{j,n\}) + \epsilon_r)\mathrm{d}\epsilon_r \quad (11)$$

Given that $P(\epsilon_r;T)$ and $f_{vr}(\{j,n\};T_{vr})$ are sampled and taking into account that $F(\epsilon)$ acts as a reaction probability of the collision complex (i.e., the probability of giving the products), $k_r(\{T\})$ is computed approximately as

$$k_r(\{T\}) = \langle\nu\rangle_T \pi b_{max}^2 f_c\, f_r \quad (12)$$

where $f_r = N_P/N_c$, where N_P is the number of trajectories in which the collision complex is formed and decomposes into the products. Note that $N_c = N_P + N_R$, where N_R is the number of trajectories in which the collision complex decays toward the reactants. Note also that N_P includes all product-generating trajectories, independent of whether $SiOH^+ + H$ are formed from $(SiOH_2^+)^*$ or from $(HSiOH^+)^*$.

If the relative energy is selected and the molecular reactant is mostly in a particular rovibrational state, that situation would correspond to the following expression

$$k_r(\epsilon_r,\{j,n\}) = k_c(\epsilon_r,\{j,n\})F(\epsilon) \approx k_c(\epsilon_r,\{j,n\})\frac{1}{1+[k_{-1}(\epsilon)/(k_2(\epsilon)+k_3(\epsilon))]} \quad (13)$$

where, of course, $\epsilon = \epsilon_r + \epsilon_{vr}(\{j,n\})$ and $F(\epsilon)$ have been approximated assuming $k_{-3}(\epsilon) \ll k_4(\epsilon)$. If only the relative energy is selected, the right-hand side would become a rovibrational average.

Note that, in a RRKM picture, the ratio appearing in the denominator of the right-hand side would be $N^{\ddagger}_{Si^+ + H_2O}(\epsilon - \epsilon^{\circ}_{Si^+ + H_2O})/(N^{\ddagger}_{TS1H}(\epsilon - \epsilon^{\circ}_{TS1H}) + N^{\ddagger}_{TS12}(\epsilon - \epsilon^{\circ}_{TS12}))$, where the $\{N^{\ddagger}_i\}$ represent the number of states above the corresponding barrier. This equivalence implies that the most important aspect of the description of the PES is the position of TS12 and TS1H with respect to the reactants.

3.C. Classification of the Reaction Paths. We have tried to classify reaction events according to the areas of the PES which are reached by the trajectory and in accordance to the reaction scheme of section 3.B. All of the reactive trajectories that lead to capture reach the region of the first minimum, M1, that is, the collision complex $(SiOH_2^+)^*$.

We distinguish three paths according to the product and to the regions of the PES visited by the trajectory

$$M1 \rightarrow Si^+ + H_2O \quad \text{(Path 1)}$$

$$M1 \rightarrow [TS12, TS1H] \rightarrow SiOH^+ + H \quad \text{(Path 2)}$$

$$M1 \rightarrow [TS1H, TS12] \rightarrow M2 \rightarrow SiOH^+ + H \quad \text{(Path 3)}$$

In path 1, M1($SiOH_2^+$) is reached and dissociates back into the reactants. In path 2, the reaction takes place through TS1H, although the area of the PES corresponding to TS12 may be visited, and the Si^+-O distance may get to very large values (4 Å). Path 3 would collect the trajectories in which the product is formed by dissociation of M2 (i.e., $HSiOH^+$).

3.D. Results for Thermal Conditions. We have run two series of trajectories with the long-range potential for two temperatures, 298.15 and 100 K, in such a way that they lead to 81 captures at 298.15 K and a similar number of 93 at 100 K. As in the capture rate computations, thermal sampling has been employed as provided by VENUS 96. As said, only those trajectories leading to capture (reaching configurations with $d(Si-O) < 3.5$ Å) are selected for the direct dynamics study, which starts at $d(Si-O) \approx 10.4$ Å. Those computations have been employed to determine f_r and the lifetimes of Table 3. However, k_c and f_c have been computed with 1000 trajectories, as described in section 3.A.

It is readily seen that f_r ($=N_P/N_c$) is very small, especially in the 298.15 K case where we have just four trajectories leading to products; of course, this result limits the accuracy of the rate constant very much. The computed rate coefficient $k_r = 0.13(6) \times 10^{-9}$ cm^3 s^{-1} is quite close to the lower bound of the experimental rate ($0.23 \pm 0.09 \times 10^{-9}$ cm^3 s^{-1}),[1,5] which is also considerably uncertain (Wlodek et al. quantify the error as 30%[5]). However, applying the electronic factor $f_e = 2/3$, the disagreement would get worse, although the error intervals would still overlap; we would have $k_r = 0.09(6) \times 10^{-9}$ cm^3 s^{-1} (298.15 K). There is a substantial increase of f_r with decreasing temperature; therefore, one gets a much larger k_r for 100 K than that for 298.15 K.

It must be noted that trajectories have been tested for zero-point energy (ZPE) leaking (see, for example, refs 35−38 and the references cited therein) by checking that the products (i.e., $SiOH^+$ in reactive trajectories and H_2O in nonreactive ones) possess a vibrational energy larger than the corresponding ZPE. All trajectories appeared to meet that criterion, which is not very surprising given that the reaction is exoergic[39] and it basically consists of an energy transfer from the relative translation of the collision into the normal modes of water.

TABLE 3: Thermal Conditions Results; f_c Represents the Ratio of Trajectories Leading to Capture, f_r is the Fraction of the Collision Complexes Which Evolve into the Products ($SiOH^+(^1\Sigma^+) + H(^2S)$), and τ Represents the "Lifetime" of the Capture Complex in the Reactive Trajectories. The Statistical Errors of the Sampling Procedure Are Given in Parentheses[33]

	100 K	298.15 K
f_c	0.431(15)	0.184(12)
k_c[a]	3.57(13)	2.61(17)
f_r	0.13(3)	0.05(2)
k_r[a,c]	0.46(11)	0.13(6)
t(fs)[b]	570(190)	260(110)

[a] Values in units of 10^{-9} cm^3 s^{-1}, and $k_r = k_c f_r$. [b] $\tau = <t_1 - t_0>$, where t_0 represents the time when it first happens that $d(Si-O) < 2$ Å, and t_1 is the time when min($d(Si-H)$, $d(O-H)$) > 3 Å, where H is the hydrogen being eliminated.

What is clear is that the shape of the PES with the two critical transition states being quite close in energy to the reactants must be the main reason for the reaction rate being so much smaller than the capture rate. There could be several reasons for the discrepancy of our computed 298 K reaction rate with the experimental value. The most obvious is, of course, the limited accuracy of f_r due to the small total number of trajectories and the fact that the flux into products is so low. Tunneling could also increase the dissociation and isomerization rates (k_2 and k_3). The fact that f_r varies so much with a relatively small decrease in temperature also points to a critical role of the position of TS12 and TS1H on the PES with respect to the reactants; note that the BHandHLYP/6-31G(d,p) levels place them a little to high.

At 100 K, the reactive trajectories are evenly split between paths 2 and 3, and our measure of the lifetime of the collision complex (which includes both M1 and M2) is about 570 ps. The "lifetimes" of Table 3 are time differences between the instant when $d(Si-O)$ first gets <2 Å to the time where min($d(Si-H)$, $d(O-H)$) > 3 Å, H representing the hydrogen atom being eliminated. We cannot reliably quantify the ratio between the numbers of the path 2 and path 3 trajectories in the 298.15 K case; we will just note that we got 3/1.

3.E. Other Results: the Effect of Translational Energy and Rovibrational Excitation. Table 4 presents f_r values computed with sets of 33 trajectories for different conditions, which are described through the translational and vibrational temperatures as well as the quantum numbers of the normal modes of water. It is readily seen that a moderate rotational excitation ($T_r = 100$ K) does not appear to have a relevant effect. However, simple excitation ($n_i = 1$) of the stretching normal modes increases f_r very substantially and a little more intensely in the case of the asymmetric stretch. Excitation of the bending movement has a negative effect. Moreover, combining the asymmetric stretch and the bending excitations ((0,1,1) vibrational state) results in a lower f_r than that of the asymmetric stretch excitation alone. Doubling the excitation quanta of the asymmetric stretch ((0,0,2) state) also doubles f_r with respect to the (0,0,1) value.

Finally the f_r value corresponding to $\epsilon_r = 11.6$ kJ/mol is zero in our computation, showing, together with the results of Table

TABLE 4: Ratio of Collision Complexes f_r Which Evolve into Products ($SiOH^+(^1\Sigma^+) + H(^2S)$) Computed under a Variety of Collision Conditions. ϵ_r (kJ/mol) and T_r Represent the Rotational Temperature, Respectively; the Vibrational State Is Described through Quantum Numbers, and Statistical Errors Are Given in Parentheses[33]

ϵ_r	T_r	Vib. State[b]	f_r
11.6	0	(0,0,0)	0
1.06	0	(0,0,0)	0.09(5)
1.06	100[a]	(0,0,0)	0.09(5)
1.06	0	(0,0,1)	0.17(7)
1.06	0	(1,0,0)	0.14(6)
1.06	0	(0,1,0)	0.04(3)
1.06	0	(0,0,2)	0.35(8)
1.06	0	(0,1,1)	0.13(6)

[a] The rotational energy corresponds to $RT_r/2$ about each rotational axis. [b] The first quantum numbers correspond to a symmetric stretch (first), bend (second), and asymmetric stretch (third).

3, that there is a sharp decrease with an increasing translational energy. The existence of a such a decrease is basically in agreement with the SIFDT experiments of Lindinger's group;[7] however, our f_r values are substantially lower than those inferred from Lindinger's data. For instance, for $\epsilon_r = 11.6$ kJ/mol, we have $f_r \approx 0$. According to Wannier's expression,[40] the latter results should be approximately comparable to the SIFDT data corresponding to $KE_{CM} = 0.12$ eV, where they have approximately 0.5 (see Figure 9 of ref 7). Our thermal 298 K value (see Table 3) is 0.05, whereas their $KE_{CM} = 0.04$ eV value (also from Figure 9) is approximately 0.96. Two reasons may explain these discrepancies. First, our computations are probably giving f_r values that are a little too low, and second, and much more important, there is a not such an evident difference between the meaning of f_r in the present paper and that of Lindinger. Their results are obtained by fitting of the experimental reaction rates k_r obtained for several KE_{CM} values to the following expression $k_r = \beta k_0/(1 + (KE_{CM}/KE_{CM1})^m)$, where k_0, KE_{CM1}, and m are parameters and β is a known function of KE_{CM} (which is nearly 1 in the present case).[7] Although βk_0 is intended to be an effective capture rate, the fitting makes it become the (limiting) low-KE_{CM} reaction rate constant. In other words, when our f_r values correct the capture rate according to eqs 12 and 13, Lindinger's, in fact, correct the low-KE_{CM} reaction rate. For that reason, we believe that our N_R/N_P values could be a better measure of $k_{-1}(\epsilon)/(k_2(\epsilon) + k_3(\epsilon))$ than the $(KE_{CM}/KE_{CM1})^m$ values inferred from SIFDT experiments, even if ours are probably too low.

3.F. Reaction Paths and Lifetimes of the $SiOH_2^+$ Complex. The fragmentation of the $SiOH_2^+$ complex into $SiOH^+ + H$ should follow, in principle, either path 2 or path 3. Also, as in the case of the $C^+ + H_2O$ reaction,[10,13] one can distinguish between direct trajectories, where the collision complex is very short-lived, and indirect ones, where it may survive many vibrational periods of the O−H or Si−H bonds before it breaks. Both kinds are compatible with path 2 and path 3. However, the distinction between both paths is not always clean because, in some trajectories, fragmentation occurs from the area of TS12-M2, but one cannot quite consider that M2 is really formed (the Si−H bond does not undergo several vibrations, as one would require).

The resulting trajectory types are presented through four examples (to some extent, they are extreme cases) in Figures 4−7, in which the variation with time of the distances between the departing hydrogen atom and both Si and O, as well as that of the Si−O distance, are displayed.

Figure 4 displays a trajectory with a long-lived intermediate corresponding to path 2. It is readily seen that a M1 → M2 isomerization almost takes place at about 930 fs. After that, the O−H bond vibrates with increasing amplitude while the Si−O distance diminishes until hydrogen is expelled.

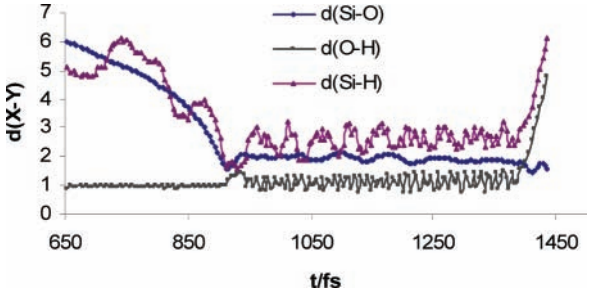

Figure 4. Variation of the Si−O, O−H, and Si−H distances (Å) with time (fs) in a slow collision on path 2.

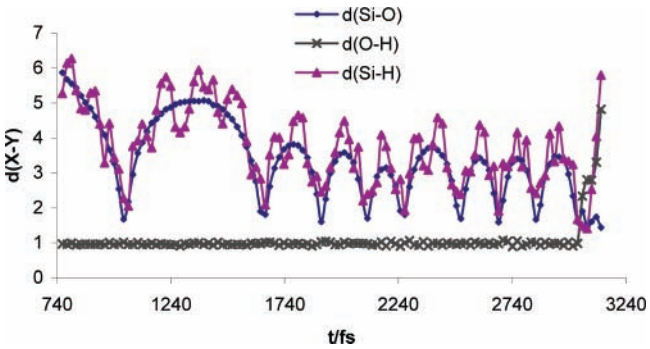

Figure 5. Variation of the Si−O, O−H, and Si−H distances (Å) with time (fs) in a slow collision on path 3.

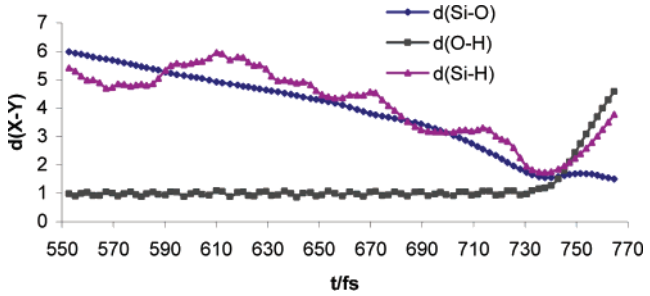

Figure 6. Variation of the Si−O, O−H, and Si−H distances (Å) with time (fs) in a fast collision on path 2.

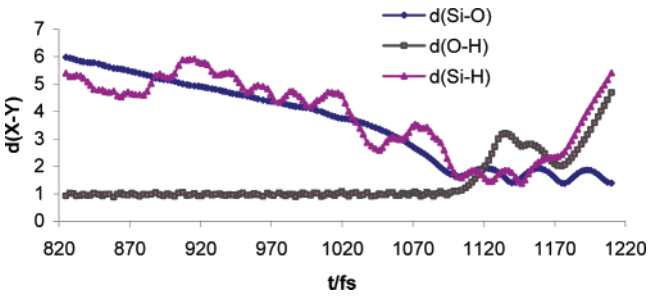

Figure 7. Variation of the Si−O, O−H, and Si−H distances (Å) with time (fs) in a fast collision on path 3.

Figure 5 displays a slow trajectory in which the area of M2 is reached; therefore, it could be assigned to path 3. The Si−O distance experiences large amplitude oscillations until it gets small enough to prompt the M1 → M2 isomerization, which, in this case, is followed immediately by a H−Si bond cleavage process. In both cases (Figures 4 and 5), it seems necessary that the Si−O bond is contracted strongly enough. In the first case (path 2), the lifetime of the collision complex (450 fs) is small compared to that of the second (about 2 ps).

Figures 6 and 7 show trajectories with short-lived complexes. Figure 6 corresponds to path 2, although it is also a borderline case where hydrogen gets quite close to Si before it departs. The fact that TS12 lies almost 6 kcal/mol below TS1H explains why hydrogen usually tilts toward Si before getting away from $SiOH^+$. In the trajectory of Figure 6, the whole process takes place in about 30 fs. In Figure 7, a "true" M1 → M2 isomerization takes place (note that the Si−H bond expends a couple of vibrational periods before it breaks). Note that, when the elimination is going to happen, hydrogen tilts back toward oxygen so that the area of TS12 is again reached. Even though the process takes about 100 fs, three times longer than that in the case of Figure 6, it is still 20 times faster than that in the case of Figure 5.

Trajectories with relatively short-lived intermediates tend to appear more often with vibrationally excited water but also account for about 40−50% of the reactive trajectories in the case of thermal samplings (100 and 298.15 K). Among them, those corresponding to the pattern of Figure 6, in which no Si−H vibration occurs even when hydrogen gets as close to Si as the Si−H equilibrium bond distance in M2, are the dominant type.

4. Conclusions

The dynamics of the $Si^+ + H_2O$ reaction, which is of major astrophysical and atmospheric significance, has been studied through quasiclassical trajectories. The method combines the use of an accurate long-range analytical potential for the study of the capture process and a direct dynamics approach to analyze the evolution of the collision complex in the case of trajectories leading to capture.

The $Si^+ + H_2O$ reaction is a very unusual case because the experimental rate coefficient is about 10 times lower than the computed capture coefficient, while, usually, simple ion−molecule reactions take place at the capture rate or at the capture rate corrected by an electronic factor. We have studied the behavior of the lowest-lying electronic states for a decreasing Si−O distance at the AQCC/aug-cc-pVTZ level; the results suggest that the electronic factor should be 2/3.

Our computed capture coefficient varies with temperature approximately as $T^{-0.8}$, and the 298 K value is in agreement or somewhat larger than previous theoretical results. The analysis of the evolution of the collision complex on the electronic ground state indicates that the low fragmentation rate into the products ($SiOH^+ + H$) as compared to that of dissociation into reactants, that is, the low (N_P/N_R) ratio, could be the only important cause of the small reaction rate. However, our 298 K reaction rate ($0.13(6) \times 10^{-9}$ cm^3 s^{-1}) is somewhat lower than the experimental result ($0.23 \pm 0.09 \times 10^{-9}$ cm^3 s^{-1}). Although other effects cannot be discarded, it is the author's opinion that the inaccuracies of the BHandHLYP/6-31G(d,p) level used in the direct dynamics computations, which are likely to favor dissociation of the collision complex into the reactants, could be responsible for most of the difference.

The present computations also show that N_P/N_R decreases quite rapidly with the translational relative energy of the reactants, being negligible at 11.6 kJ/mol. We also conclude that moderate rotational excitation ($T_r = 100$ K) does not have a noticeable effect on N_P/N_R. However, excitation of the symmetric and asymmetric stretching modes by even one quantum substantially increases N_P/N_R.

Reactive trajectories can be classified roughly as "direct", where the collision complex is very short-lived, and "indirect", where it could survive for hundreds of femtoseconds or longer than 1 ps. In most trajectories, especially in the case of the direct ones, the products originate from $SiOH_2^+$, even if the area of $HSiOH^+$ is visited during the O−H bond breaking process. However, it is not infrequent that a true $SiOH_2^+ \rightarrow HSiOH^+$ isomerization takes place, where the latter species undergoes a number of Si−H vibrations before fragmentation. Vibrational excitation of the stretching normal modes of water tends to favor direct trajectories and $SiOH_2^+$ as the only intermediate.

Acknowledgment. I am indebted to Professor William Hase for giving permission to interface my routines to Venus 96 in order to carry out the QCT capture computations. I acknowledge the financial support of the Xunta de Galicia through the Project PGIDT05PXIB31402PR. The services provided by the "Centro de Supercomputación de Galicia" (CESGA) and, in particular, the assistance of Carlos Fernandez are acknowledged.

Appendix A

The ion−dipole attraction potential is represented as follows

$$V_q = \frac{1}{4}\frac{\delta q_O e^2}{\pi\epsilon_0 r_1} + \frac{1}{4}\frac{\delta q_H e^2}{\pi\epsilon_0 r_2}\frac{1}{4}\frac{\delta q_H e^2}{\pi\epsilon_0 r_3} \tag{A1}$$

where r_1, r_2, and r_3 are the d(Si−O), d(Si−H_1), and d(Si−H_2) distances. V_r is a repulsive part, which is given the following form

$$V_r = \frac{A_O}{(r_1 - \delta r_1)^{10}} + \frac{A_H}{r_2^{10}} + \frac{A_H}{r_3^{10}} \tag{A2}$$

and V_L includes the following attractive terms

$$V_L = -\frac{A_L}{(r_1 + \delta r_B)^4} - \frac{B_L}{(r_1 + \delta r_B)^6} \tag{A3}$$

V_i is the internal potential of the water molecule, which is made dependent on the Si−O distance

$$V_i = V_{OH_1} + V_{OH_2} + V_{bend} \tag{A4}$$

We have

$$V_{OH_1} = D_{OH}(r_1,r_5)(1 - e^{-\beta(r_1,r_5)(r_4 - r_{eq})})^2 \tag{A5}$$

where r_4 and r_5 are the d(O−H_1) and d(O−H_2) distances. The dissociation energy is written as follows

$$D_{OH}(r_1,r_5) = E_{OH}/f_s(r_5 - r_{eq}(r_1)) + (1 + f_d(r_5))\left(\sum_{i=1<bu>4} \frac{d_i}{(r_1 - r_{1,x}(r_5,r_1))^i}\right) \tag{A6}$$

with

$$r_{eq}(r_1) = d(O-H)_{eq} + A_{eq}/{r_1}^2$$
$$f_d(r_5) = B_1(r_5 - r_{eq}(r_1))$$
$$f_d = 1 + C_1(r_5 - r_{eq}(r_1))$$
$$r_{1,x}(r_5) = d(SiO_x) - A_x(r_5 - r_{eq}(r_1)) \tag{A7}$$

where d(O−H)$_{eq}$ is the equilibrium bond distance, A_{eq}, B_1, C_1, d(SiO_x), and A_x are parameters, and $\beta(r_1,r_5)$ is given the following expression

$$\beta(r_1,r_5) = \beta_0 + \frac{B_\beta}{r_1^3} - B_0(r_5 - \delta\mathrm{OH}) \qquad \text{(A8)}$$

V_{OH_2} has an equivalent expression in terms of r_5 and $D_{OH}(r_1,r_4)$. Finally, V_{bend} is represented as follows

$$V_{bend} = g(r_4)g(r_5)h(r_1)\sum_{k=1}^{m} b_k(a - a_{eq})^{k+1} \qquad \text{(A9)}$$

with $m = 3$

$$h(r_1) = 1 + \sum_{i=2}^{4} h_i/(r_1 - \delta\mathrm{CO}_h)^i \qquad \text{(A10)}$$

and

$$g(r_4) = 1 + \sum_{l=1}^{3} g_l(r_4 - r_{eq}(r_1))^1 \qquad \text{(A11)}$$

The values of the parameters are presented in the Supporting Information (Table S1).

Supporting Information Available: The parameters of the long-range potential described in Appendix A are given in Table S1. This material is available free of charge via the Internet at http://pubs.acs.org.

References and Notes

(1) Fahey, D. W.; Fehsenfeld, F. C.; Ferguson, E. E.; Viehland, L. A. *J. Chem. Phys.* **1981**, *75*, 669.
(2) Turner, J. L.; Dalgarno, A. *Astrophys. J.* **1977**, *213*, 386.
(3) Millar, T. J. *Astrophys. Space Sci.* **1980**, *72*, 509.
(4) Clegg, R. E. S.; van Izendoorn, J. L.; Allamandola, L. J. *Mon. Not. R. Astron. Soc.* **1983**, *203*, 105.
(5) Wlodek, S.; Fox, A.; Bohme, D. K. *J. Am. Chem. Soc*. **1987**, *109*, 6663.
(6) Su, T.; Chesnavich, W. J. *J. Chem. Phys.* **1982**, *76*, 5183.
(7) Glosík, J.; Zakouřil, P.; Lindinger, W. *J. Chem. Phys.* **1995**, *103*, 6490.
(8) González, A. I.; Clary, D. C.; Yáñez. M. *Theor. Chim. Acta* **1997**, *98*, 33.
(9) Ishikawa, Y.; Binning, R. C., Jr.; Ikegami, T. *Chem. Phys. Lett.* **2001**, *343*, 413.
(10) Ishikawa, Y.; Ikegami, T.; Binning, R. C., Jr. *Chem. Phys. Lett.* **2003**, *370*, 490.
(11) Flores, J. R. *J. Chem. Phys.* **2006**, *125*, 164309.
(12) Clary, D. C.; Dateo, C. E.; Smith, D. *Chem. Phys. Lett.* **1993**, *22*, 1469.
(13) Flores, J. R. *J. Phys. Chem.* **1992**, *96*, 4414.
(14) Curtiss, L. A.; Raghavachari, K.; Redfern, P. C.; Rassolov, V.; Pople, J. A. *J. Chem. Phys.* **1998**, *109*, 7764.
(15) Szalay, P. G.; Bartlett, R. J. *Chem. Phys. Lett*. **1993**, *214*, 481.
(16) Kendall, R. A.; Dunning, T. H., Jr.; Harrison, R. J. *J. Chem. Phys.* **1992**, *96*, 6769.
(17) Woon, D. E.; Dunning, T. H., Jr. *J. Chem. Phys*. **1993**, *98*, 1358.
(18) Werner, H.-J.; Knowles, P. J. *J. Chem. Phys.* **1985**, *82*, 5053.
(19) Knowles, P. J.; Werner, H.-J. *Chem. Phys. Lett.* **1985**, *115*, 259.
(20) Werner H.-J.; Knowles, P. J. with contributions by Almlöf, J.; Amos, R. D.; Berning, A. MOLPRO, a package of ab initio programs; http://www.molpro.net/.
(21) Bolton, K.; Hase, W. L.; Peslherbe, G. H. Direct Dynamics Simulations in Reactive Systems. In *Modern Methods in Multidimensional Dynamics Computations in Chemistry*; Thompson, D. L., Ed.; World Scientific: Singapore, 1998.
(22) Becke, A. D. *J. Chem. Phys.* **1993**, *98*, 5648.
(23) Frisch, M. J.; Trucks, G. W.; Schlegel, H. B.; Scuseria, G. E.; Robb, M. A.; Cheeseman, J. R.; Montgomery, J. A., Jr.; Vreven, T.; Kudin, K. N.; Burant, J. C.; Millam, J. M.; Iyengar, S. S.; Tomasi, J.; Barone, V.; Mennucci, B.; Cossi, M.; Scalmani, G.; Rega, N.; Petersson, G. A.; Nakatsuji, H.; Hada, M.; Ehara, M.; Toyota, K.; Fukuda, R.; Hasegawa, J.; Ishida, M.; Nakajima, T.; Honda, Y.; Kitao, O.; Nakai, H.; Klene, M.; Li, X.; Knox, J. E.; Hratchian, H. P.; Cross, J. B.; Bakken, V.; Adamo, C.; Jaramillo, J.; Gomperts, R.; Stratmann, R. E.; Yazyev, O.; Austin, A. J.; Cammi, R.; Pomelli, C.; Ochterski, J. W.; Ayala, P. Y.; Morokuma, K.; Voth, G. A.; Salvador, P.; Dannenberg, J. J.; Zakrzewski, V. G.; Dapprich, S.; Daniels, A. D.; Strain, M. C.; Farkas, O.; Malick, D. K.; Rabuck, A. D.; Raghavachari, K.; Foresman, J. B.; Ortiz, J. V.; Cui, Q.; Baboul, A. G.; Clifford, S.; Cioslowski, J.; Stefanov, B. B.; Liu, G.; Liashenko, A.; Piskorz, P.; Komaromi, I.; Martin, R. L.; Fox, D. J.; Keith, T.; Al-Laham, M. A.; Peng, C. Y.; Nanayakkara, A.; Challacombe, M.; Gill, P. M. W.; Johnson, B.; Chen, W.; Wong, M. W.; Gonzalez, C.; Pople, J. A. *Gaussian 03*; Gaussian, Inc.: Wallingford, CT, 2004.
(24) Hehre, W. J.; Ditchfield, R.; Pople, J. A. *J. Chem. Phys.* **1972**, *56*, 2257.
(25) Francl, M. M.; Pietro, W. J.; Hehre, W. J.; Binkley, J. S.; Gordon, M. S.; DeFrees, D. J.; Pople, J. A. *J. Chem. Phys.* **1982**, *77*, 3654.
(26) McLean, A. D.; Chandler, G. S. *J. Chem. Phys.* **1980**, *72*, 5639.
(27) Vande Linde, S. R.; Hase, W. L. *J. Phys. Chem.* **1990**, *94*, 2778.
(28) Hase, W. L.; Duchovich, R. J.; Hu, X.; Komornicki, A.; Lim, K. F.; Lu, D.; Peslherbe, G. H.; Swamy, K. N.; Vande Linde, S. R.; Varandas, A.; Wang, H.; Wolf, R. Venus 96, A General Chemical Dynamics Computer Program. *QCPE Bull.* **1996**, *16*, 43.
(29) Millam, J. M.; Bakken, V.; Chen, W.; Hase, W. L.; Schlegel, H. B. *J. Chem. Phys.* **1999**, *111*, 3800.
(30) Li, X.; Millam, J. M.; Schlegel, H. B. *J. Chem. Phys.* **2000**, *113*, 10062.
(31) Press, W. H.; Vetterling, W. T.; Teukolski, S. A.; Flannery, B. P. *Numerical Recipes in Fortran 77*, 2nd ed.; Cambridge University Press: New York, 1992.
(32) Chen, W.; Hase, W. L.; Schlegel, H. B. *Chem. Phys. Lett.* **1994**, *228*, 436.
(33) Porter R. N.; Raff, L. M. In *Dynamics of Molecular Collisions*, Part B; Miller, W. H., Ed.; Plenum Press: New York, 1976; Chapter 1.
(34) Marquette, J. B.; Rowe, B. R.; Dupeyrat, G.; Poissant, G.; Rebrion, C. *Chem. Phys. Lett.* **1985**, *122*, 431.
(35) Hase, W. L.; Bukowski, D. G. *J. Comput. Chem.* **1982**, *3*, 335.
(36) Schatz, G. C. *J. Chem. Phys.* **1983**, *79*, 5386.
(37) Lu, D.-h.; Hase, W. L. *J. Chem. Phys.* **1989**, *91*, 7490.
(38) Guo, Y.; Thompson, D. L.; Sewell, T. D. *J. Chem. Phys.* **1996**, *104*, 576.
(39) Bowman, J. M.; Schatz, G. C.; Kuppermann, A. *Chem. Phys. Lett.* **1974**, *24*, 378.
(40) Viehland, L. A.; Mason, E. A. *J. Chem. Phys.* **1977**, *66*, 422.